Bias-Induced Hole Mobility Increase in Narrow [111] and [110] Si Nanowire Transistors

Neophytos Neophytou and Hans Kosina

***Abstract*—We report on the phonon-limited hole mobility of ultra-narrow Si nanowire (NW) channel transistors as a function of inversion charge density. We employ atomistic bandstructure calculations and linearized Boltzmann transport theory and examine NWs of 12 nm in diameter in [100], [110], and [111] transport orientations. We show that the curvature of the bands in the [110] and [111] NWs increases significantly as the channel is driven into inversion, which results in a ∼50% mobility increase. In the case of the [100] NW, on the other hand, such feature is not observed.**

***Index Terms*—Bandstructure, Boltzmann transport, hole mobility, Si nanowires (NWs), tight-binding (TB).**

I. Introduction

SILICON nanowires (NWs) have recently attracted significant attention as candidates for next-generation transistor devices [1], [2]. The NW gate-all-around geometry suppresses short-channel effects and reduces leakage. Recently realized narrow NW transistors have already demonstrated excellent performance [1], [2]. In addition, the strong quantum confinement can alter the electronic dispersion and, thus, the transport properties of the NW. The transport and surface orientations and the confinement length scale are additional degrees of freedom in engineering device properties. This has been demonstrated by measurements and simulations for NWs [3]–[5], as well as ultra-thin layers [6].

Specifically for p-type Si NW channels, regarding the effect of orientation, it was shown that the [111] channel is advantageous compared to the [110] channel and both are largely advantageous compared to the [100] channel [4], [5]. Regarding the confinement length scale, it was also shown that the hole velocity and mobility in these [111] and [110] channels increase significantly compared to bulk as the NW diameter scales down to ultra-narrow values $D = 3$ nm [3], [4], [7].

In this letter, we theoretically show that an increase in the mobility in [111] and [110] p-type NWs can also be observed for larger NW diameters under electrostatic confinement. As V_G increases and the channel is driven into inversion, a maximum in the mobility is observed, which can be ∼50% higher than the low-bias mobility values. As the channel is driven deeper into strong inversion, the mobility drops back to the low-bias values because the Fermi level is pushed into energy regions with larger density of states, which increases scattering. The mechanism behind this is related to bias-dependent bandstructure modifications.

Manuscript received February 2, 2012; revised February 16, 2012; accepted February 17, 2012. Date of publication April 5, 2012; date of current version April 20, 2012. This work was supported by the Austrian Climate and Energy Fund, Contract 825467. The review of this letter was arranged by Editor C. Bulucea.

The authors are with the Institute for Microelectronics, Vienna University of Technology, 1040 Vienna, Austria (e-mail: neophytou@iue.tuwien.ac.at).

Color versions of one or more of the figures in this letter are available online at http://ieeexplore.ieee.org.

Digital Object Identifier 10.1109/LED.2012.2188879

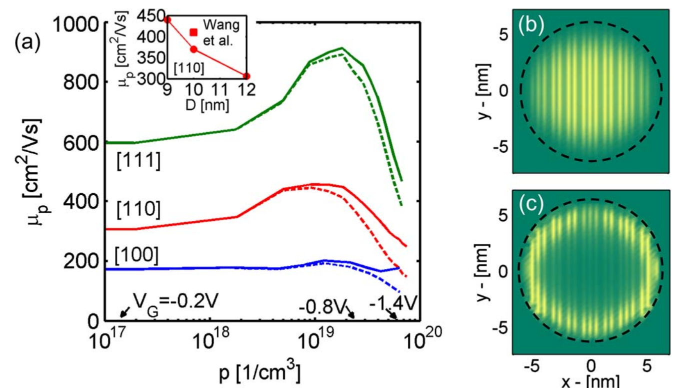

Fig. 1. Low-field hole mobility versus the total carrier concentration in the cross section of the NW. The cylindrical NWs of $D = 12$ nm in the [100], [110], and [111] transport orientations are shown. (Solid) Phonon-limited results. (Dashed) Phonon plus SRS-limited results. Three corresponding gate biases are indicated (approximate positions). (Inset) Simulation (low carrier concentration) versus experimental result from [10] (square) for the [110] NW. (b–c) Hole distribution in the cross section of the [110] NW at (a) OFF state ($V_G = -0.2$ V) and (b) inversion ($V_G = -0.8$ V).

II. Method and Results

We employ the atomistic sp^{3}d^{5}s*-spin-orbit-coupled tight-binding (TB) model [8] for electronic structure calculations and solve self-consistently the 2-D Poisson equation for the electrostatic potential in the cross section of the NW, as described in [4]. The TB model used captures the electronic structure accurately and inherently includes the effects of quantum confinement. Once the self-consistent electronic structure is obtained, the mobility is extracted using linearized Boltzmann transport theory, including phonon and surface roughness (SR) scattering (SRS), and the full energy dependence of the relaxation rates as in [7]. We consider bulk phonons with bulk deformation potential values. Although the effect of phonon confinement could have some quantitative influence [9], our conclusions are qualitatively electronic-structure related and would not be affected by the nature of phonons. Our mobility values are still in good agreement with experimental data [10] (see the inset of Fig. 1).

We simulate the low-field mobility in the cylindrical p-type NWs of $D = 12$ nm in the [100], [110], and [111] transport orientations as a function of the total charge density in the

0741-3106/$31.00 © 2012 IEEE

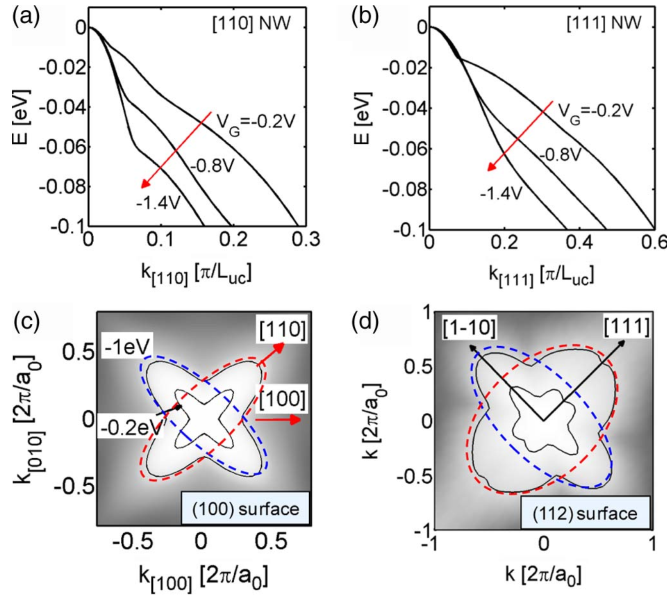

Fig. 2. (a), (b) Highest NW valence band for $-V_G = 0.2/0.8/1.4$ V for (a) the [110] and (b) the [111] NWs of $D = 12$ nm. All bands are shifted to $E = 0$ eV. (c), (d) Energy contours of the bulk Si HH valence band. (c) (100) surface. (d) (112) surface. At first order, these warped bands can be approximated by two ellipsoids with their longitudinal axes perpendicular to each other.

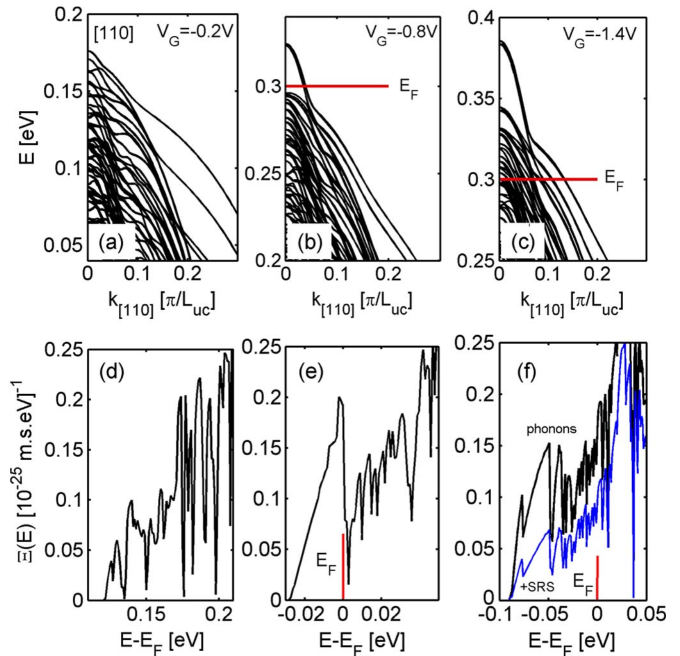

Fig. 3. Electronic dispersions for the p-type [110] NW of $D = 12$ nm under low and high gate biases. (a) OFF state: $V_G = -0.2$ V. (b) Inversion: $V_G = -0.8$ V. (c) Strong inversion: $V_G = -1.4$ V. The Fermi level is indicated. (d–f) Phonon-limited TD function versus energy for the cases (a–c). In (f), phonon-limited and phonon-plus-SRS-limited results are shown.

cross section of the NW (divided by the cross-sectional area to be converted into a 3-D density). In all NW cases, the gate insulator is assumed to be SiO_2 of thickness 1.2 nm. The results are shown in Fig. 1. A large anisotropy is observed, with the [111] NW having a $\sim 2\times$ higher mobility than the [110] NW and a $\sim 3\times$ higher mobility than the [100] NW. As the channel is driven into inversion, the phonon-limited mobility (solid lines) in the [111] and [110] NWs increases by $\sim$50% until it reaches a maximum. Afterwards, it decreases close to or even below the initial values at low carrier densities. In the case of the [100] NW, the mobility is the lowest and remains almost constant. The dashed lines in Fig. 1 show the low-field mobility including phonons plus SRS implemented as described in [9], using $\Delta_{\rm rms} = 0.48$ nm and $L_C = 1.3$ nm. The improvement in the phonon-limited mobility with channel inversion is strong enough to offset the detrimental effect of SRS which appears at concentrations beyond $p = 10^{19}/\text{cm}^3$.

The reason behind the mobility increase for the [111] and [110] NWs is explained in Fig. 1(b) and (c), which shows the hole density distribution in the cross section of the [110] NW under low and high carrier concentrations (at $V_G = -0.2$ V and $V_G = -0.8$ V, respectively). The latter case is close to the mobility maximum. At low V_G, the hole density is located in the entire volume of the channel, and as V_G increases, it shifts toward the surface. This electrostatic carrier confinement, however, results in a strong variation in the curvature of the subbands. Fig. 2(a) shows the change in the highest valence subband of the [110] NW for different V_G's. For $V_G = -0.2$ V, when the electrostatic potential in the cross section of the NW is almost flat, the dispersion has a small curvature. As V_G increases, the dispersion acquires a larger curvature, which results in higher carrier velocities, less final states for scattering, and, finally, higher mobility, which explains the increase observed in Fig. 1. A very similar observation is made for the subbands of the [111] NW as well [Fig. 2(b)]. We note that this subband behavior is observed for these two NWs also under diameter scaling [4], [7], but here, we show that electrostatic confinement can have a similar effect. The explanation for this effect originates from the warped shape of the heavy-hole (HH) valence band as shown in Fig. 2(c) and (d). At first order, confinement can be thought of as introducing larger curvature bands from Brillouin-zone regions away from the center, similar to the "particle in a box" quantization picture as we explain in [4]. Alternatively, one can think that the HH consists of two ellipsoids rotated at 90° to each other (Fig. 2(c) and (d) corresponds to the relevant surfaces for the [110] and [111] NWs, respectively) [11]. Electrostatic confinement by a (110) surface shifts the lightly confined valley (red) away from the initial ground state. The dispersion along the [110] or [111] transport directions is then formed from the light subbands of the other valley (blue). Beyond the band shifts, electrostatic confinement introduces additional warping of the bands.

After the mobility of the [111] and [110] NWs reaches a maximum of around $p = 2 \times 10^{19}/\text{cm}^3$, it then starts to drop. To understand this, Fig. 3(a)–(c) shows the electronic structures of the [110] NW at $(-V_G) = 0.2/0.8/1.4$ V, respectively. For the dispersion of Fig. 3(a), the electrostatic potential in the cross section of the NW is almost flat. Under inversion conditions [Fig. 3(b)], the Fermi level is pushed into the subbands, which now have a larger curvature, something also reported for thin layers [12]. As $(-V_G)$ increases and the channel is driven into a deeper strong inversion, the Fermi level is pushed even deeper into the subbands [Fig. 3(c)]. The number of subbands that participate in transport is now increased, and their masses are

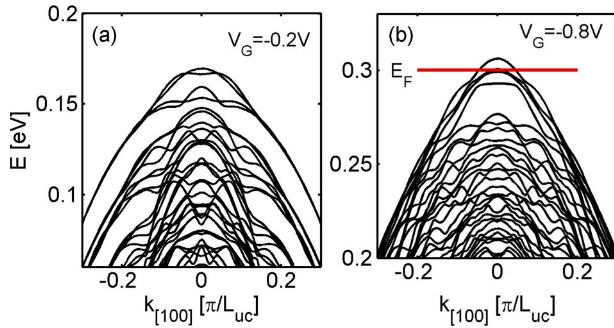

Fig. 4. Electronic dispersions for the p-type [100] NW of $D = 12$ nm under low and high gate biases. (a) OFF state: $V_G = -0.2$ V. (b) Inversion: $V_G = -0.8$ V.

heavier, which reduces the mobility. The mobility reduction is more clearly understood from the transport distribution function (TD) which is defined as [7]

$$\Xi(E) = \sum_{k_x,n} v_n^2(k_x)\tau_n(k_x)\delta\left(E - E_n(k_x)\right). \quad (1)$$

This function determines the mobility via the definition

$$\mu_p = \frac{q_0}{p}\int_{E_v}^{-\infty} dE\left(-\frac{\partial f_0}{\partial E}\right)\Xi(E). \quad (2)$$

Both the carriers' velocity $v_n(k_x)$ and relaxation time $\tau_n(k_x)$ decrease as the subband mass and the density of the final scattering states increase. The TDs for the cases corresponding to the dispersions of Fig. 3(a)–(c) are shown in Fig. 3(d)–(f). The amplitude of the TD around the Fermi level at $V_G = -0.8$ V is higher than in the other cases, which justifies the shape of the mobility in Fig. 1. Fig. 3(f) also indicates how the TD is reduced when SRS is included (blue).

The mobility for the [100] NW, on the other hand, does not increase with inversion. Fig. 4 shows the [100] NW dispersions for $(-V_G) = 0.2/0.8$ V. The curvature and shape of the bands are not strongly affected by V_G. Therefore, the mobility is not affected either. In addition, the strong oscillatory shape of the bands keeps the group velocity low, which results in the lowest mobility values.

Because the mobility trends with bias and orientation in Fig. 1 originate from the shape of the HH band, we mention that similar effects should be observed for p-type semiconductors other than Si as well. Note that at smaller diameters, the magnitude of the bias-induced increase we describe is reduced since the bands are already quantized by physical confinement. The increase drops to 25% at $D = 9$ nm and is unnoticeable at $D = 6$ nm. Another point worth mentioning is that for short-channel devices that operate close to the ballistic limit, mobility loses its relevance and it is limited to a few hundred cm^2/V-s, even for very high-mobility channels [5], [13], [14]. However, the bandstructure effects that improve the intrinsic channel performance lead to increased mean free paths for scattering, which increases the channel ballisticity [15] and the transistor's speed.

III. Conclusion

In summary, we have investigated the effect of the electrostatic confinement on the low-field mobility of p-type Si NWs of 12 nm in diameter. We used atomistic dispersions, self-consistently calculated with electrostatics, and linearized Boltzmann transport theory. As the holes are electrostatically confined near the surface of the NW, their bands become lighter. This increases the mobility of the [111] and [110] NWs by ~50%. It is, therefore, possible to achieve an improved mobility as the channel is driven into inversion, even at the presence of SRS, and, thus, an improved transistor speed.

References

[1] S. D. Suk, M. Li, Y. Y. Yeoh, K. H. Yeo, K. H. Cho, I. K. Ku, H. Cho, W. J. Jang, D.-W. Kim, D. Park, and W.-S. Lee, "Investigation of nanowire size dependency on TSNWFET," in *Proc. IEEE IEDM*, 2007, pp. 891–894.

[2] S. Bangsaruntip, G. M. Cohen, A. Majumdar, Y. Zhang, S. U. Engelmann, N. C. M. Fuller, L. M. Gignac, S. Mittal, J. S. Newbury, M. Guillorn, T. Barwicz, L. Sekaric, M. M. Frank, and J. W. Sleight, "High performance and highly uniform gate-all-around silicon nanowire MOSFETs with wire size dependent scaling," in *Proc. IEEE IEDM*, 2009, pp. 1–4.

[3] K. Trivedi, H. Yuk, H. C. Floresca, M. J. Kim, and W. Hu, "Quantum confinement induced performance enhancement in sub-5-nm lithographic Si nanowire transistors," *Nano Lett.*, vol. 11, no. 4, pp. 1412–1417, Apr. 2011.

[4] N. Neophytou, A. Paul, and G. Klimeck, "Bandstructure effects in silicon nanowire hole transport," *IEEE Trans. Nanotechnol.*, vol. 7, no. 6, pp. 710–719, Nov. 2008.

[5] M. Luisier and G. Klimeck, "Phonon-limited mobility and injection velocity in n- and p-doped ultrascaled nanowire field-effect transistors with different crystal orientations," in *Proc. IEEE IEDM*, 2010, pp. 861–864.

[6] G. Tsutsui, M. Saitoh, and T. Hiramoto, "Experimental study on superior mobility in [110]-oriented UTB SOI pMOSFETs," *IEEE Electron Device Lett.*, vol. 26, no. 11, pp. 836–838, Nov. 2005.

[7] N. Neophytou and H. Kosina, "Atomistic simulations of low-field mobility in Si nanowires: Influence of confinement and orientation," *Phys. Rev. B, Condens. Matter*, vol. 84, no. 8, pp. 085313-1–085313-15, Aug. 2011.

[8] T. B. Boykin, G. Klimeck, and F. Oyafuso, "Valence band effective-mass expressions in the $\mathrm{sp}^3\mathrm{d}^5\mathrm{s}^*$ empirical tight-binding model applied to a Si and Ge parametrization," *Phys. Rev. B*, vol. 69, no. 11, p. 115 201, Mar. 2004.

[9] E. B. Ramayya, D. Vasileska, S. M. Goodnick, and I. Knezevic, "Electron transport in silicon nanowires: The role of acoustic phonon confinement and surface roughness scattering," *J. Appl. Phys.*, vol. 104, no. 6, pp. 063711-1–063711-12, Sep. 2008.

[10] R. Wang, H. Liu, R. Huang, J. Zhuge, L. Zhang, D.-W. Kim, X. Zhang, D. Park, and Y. Wang, "Experimental investigations on carrier transport in Si nanowire transistors: Ballistic efficiency and apparent mobility," *IEEE Trans. Electron Devices*, vol. 55, no. 11, pp. 2960–2967, Nov. 2008.

[11] E. X. Wang, P. Matagne, L. Shifren, B. Obradovic, R. Kotlyar, S. Cea, M. Stettler, and M. Giles, "Physics of hole transport in strained silicon MOSFET inversion layers," *IEEE Trans. Electron Devices*, vol. 53, no. 8, pp. 1840–1851, Aug. 2006.

[12] L. Donetti, F. Gámiz, S. Thomas, T. E. Whall, D. R. Leadley, P.-E. Hellström, G. Malm, and M. Östling, "Hole effective mass in silicon inversion layers with different substrate orientations and channel directions," *J. Appl. Phys.*, vol. 110, no. 6, pp. 063711-1–063711-8, Sep. 2011.

[13] N. Neophytou, T. Rakshit, and M. Lundstrom, "Performance analysis of 60-nm gate-length III–V InGaAs HEMTs: Simulations versus experiments," *IEEE Trans. Electron Devices*, vol. 56, no. 7, pp. 1377–1387, Jul. 2009.

[14] E. Gnani, A. Gnudi, S. Reggiani, and G. Baccarani, "Effective mobility in nanowire FETs under quasi-ballistic conditions," *IEEE Trans. Electron Devices*, vol. 57, no. 1, pp. 336–344, Jan. 2010.

[15] C. Jeong, D. A. Antoniadis, and M. S. Lundstrom, "On backscattering and mobility in nanoscale silicon MOSFETs," *IEEE Trans. Electron Devices*, vol. 56, no. 11, pp. 2762–2769, Nov. 2009.